Microwave Radiative Transfer in the Mixed-Phase Regions of Tropical Rainfall

T. T. WILHEIT

Department of Atmospheric Science, Texas A&M University, College Station, Texas

P. V. HOBBS*

Atmospheric Sciences Department, University of Washington, Seattle, Washington

K. JIN+

Department of Atmospheric Science, Texas A&M University, College Station, Texas

A. L. RANGNO

Atmospheric Sciences Department, University of Washington, Seattle, Washington

M. E. TRIESKY AND J. R. WANG

NASA Goddard Space Flight Center, Greenbelt, Maryland

(Manuscript received 29 November 2005, in final form 10 April 2006)

ABSTRACT

Here airborne observations of the mixed-phase regions of tropical oceanic rainfall are reported as part of the Kwajalein Experiment. The University of Washington Convair-580 aircraft carrying upward-viewing 21- and 37-GHz microwave radiometers spiraled down through stratiform rain. It was observed that the microwave absorption coefficient in the bright band (melting layer) in the stratiform rainfall was roughly twice or thrice that of the rain below. Radiative transfer models of the melting layer have a similar range of uncertainties. In addition to the potential bias from modeling uncertainties, comparison with previous observations suggests that there is a natural variability of about the same magnitude.

The aircraft also made penetrations of a convective line at altitudes of 2.6, 3.4, and 4.5 km. From the microwave observations, it can be concluded that the effect of supercooled water above the freezing level was extremely small, on the order of 2% or less of the total rain signal for this case.

1. Introduction

It would be difficult to overstate the importance of tropical rainfall. The latent heat that it releases drives the largest scales of atmospheric circulation, and the freshwater input it provides is a major factor in the thermohaline circulation of the oceans. Thus, quantitative understanding of the weather and climate system of the earth requires similarly quantitative understanding of tropical rainfall. The measurement of tropical oceanic rainfall, with which this paper is concerned, is difficult. Most of the Tropics are ocean covered with the attendant logistical difficulties in making conventional rainfall measurements. Land areas have their own set of difficulties. The only practical approach to measure rainfall throughout the Tropics is to use satellite-based measurements. Passive microwave measurements have many advantages for this measurement and are applied on the Tropical Rainfall Measuring Mission (TRMM) satellite via the TRMM Microwave Imager (TMI) and on the *Aqua* satellite via the Advanced Microwave

* Deceased.

+ Current affiliation: NASA JPL, California Institute of Technology, Pasadena, California.

Corresponding author address: Dr. T. T. Wilheit, Department of Atmospheric Science (3150), Texas A&M University, College Station, TX 77843-3150.
E-mail: wilheit@tamu.edu

Scanning Radiometer (AMSR-E; Kummerow et al. 1998; Kawanishi et al. 2003; Wilheit et al. 2003)

The original TRMM Level-2 (Kummerow et al. 2001) and Level-3 (Chang et al. 1999) algorithms treated the hydrometeors as being all liquid below the freezing level (0°C isotherm). The Level-3 algorithm treats the hydrometeors as all frozen above the freezing level and assumes that their impact is negligible at the frequencies being used (19.35 and 21.3 GHz). Clearly, this is too simple. In stratiform rain, the falling snow melts over some distance after it passes the freezing level causing the familiar radar bright band, and some supercooled water is advected above the freezing level in updrafts, especially in convective precipitation.

There has been considerable effort in recent years (Bauer et al. 1999, 2000; Bauer 2001; Olson et al. 2001a,b) to model the radiometric impact of the melting layer of stratiform rain. These models use 1D and 2D nonhydrostatic cloud models, thermodynamic models of the melting process, and various electromagnetic models of the mixed-phase particles to compute the absorption and scattering within the melting layer. Also, Liang and Meneghini (2005) have performed detailed electromagnetic calculations of the radar reflectivity of the melting layer. Each model includes a mixture of first principles modeling and parameterization. Since there is a range of choices for the parameterizations, the results vary. Generally, the results suggest an increase in the absorption and extinction coefficients within the melting layer. At 37 GHz over the typical 0.5-km thickness of the melting layer, these coefficients are 2–3 times their values within the fully melted rain layer below, reflecting the range of mixed media parameterizations used to calculate the bulk dielectric properties of the droplets. At lower frequencies, the ratio of the absorption in the melting layer to that of the rain below is larger with a great deal of variability depending on the mixed media parameterization.

Although the nominal measurement of the precipitation radar (PR) on TRMM is backscatter strength (Z), proper interpretation requires an attenuation correction because of moderately strong attenuation at 13.8 GHz. This process is described by Iguchi et al. (2000). They assume a relationship between the attenuation coefficient (k) and Z of the form $k = \alpha Z^{\beta}$, where β is in the range of 0.77–0.8 depending on the assumed drop size distribution (DSD). This inherently results in an increase in attenuation in the bright band. For typical bright bands, the excess attenuation is of the order of a factor of 2 or 3 above the attenuation of the fully melted rain below, essentially the same as one would infer for the 37-GHz attenuation based on the models mentioned above rather than the even greater increased attenuation one would infer from the frequency dependence of the modeling studies discussed above.

In an effort to verify the effect of the bright band on microwave radiances, Bauer (2001) located 48 events in TRMM PR data that contained identifiable bright bands. He ran simulations appropriate to these cases using three cloud-resolving models, the Goddard Cumulus Ensemble Model-1 (GCE-1), the Goddard Cumulus Ensemble Model-3 (GCE-3), and the Meteo-France Large Eddy Model CETP (Meso-NH). Each model was run both with and without his melting layer model included and radiative transfer calculations were performed for the TRMM Microwave Imager viewing parameters. He used the radar data to partition the TMI observations into stratiform rain with a bright band and stratiform rain without a bright band. He then compared the probability distribution functions for the brightness temperatures from the simulations and the observations both with and without a bright band. The GCE-1 results are typical. At 10.7 GHz, many more high brightness temperatures (>200 K) were observed than simulated, but the presence of the bright band seemed to increase the brightness temperature in both the simulations and the observations by similar amounts. At 19.35 GHz, the observed range of brightness temperatures is greater than simulated. The observed bright band effect is negative for brightness temperatures less than about 200 K and much greater than simulated above 200 K. At 37 GHz, the simulated brightband effect is small and the observed brightband effect is negative. The ranges of the brightness temperatures are reasonably consistent between the simulations and the observations. At 85.5 GHz, the simulated brightband effect is very small and the observed effect is large in magnitude but negative. There were essentially no observations below 200 K, but about 10% of the simulated brightness temperatures were below this value. As is often observed, the simulations give much more scattering by ice than is observed over the oceans, but this is a separate issue. Since spaceborne radiometers measure an integrated effect of the entire rain column and the surface, quantitative interpretation of these observations is a challenge.

More direct observations are difficult and infrequent. Two measurements were reported by Chang et al. (1993) in stratiform rain. As with this paper, there were no radar observations to support the presence or absence of a bright band. This paper adds to the very sparse observational database of the radiometric effects of the melting layer.

Radiometric observations of the effects of super-

cooled water in updrafts likewise are scarce. Aircraft safety considerations make an already difficult observation even more so. A token amount of emission, presumably from supercooled water, was reported by Chang et al. (1993); the authors are not aware of any other observations. This paper reports an upper limit to the supercooled water that could have been present in a convective rainfall event.

2. The experiment

The TRMM Kwajalein Experiment (KWAJEX) was one of a series of field campaigns for the testing of rainfall retrievals from the TRMM satellite and the only one specifically directed toward oceanic rainfall retrievals. The experiment was carried out near the Kwajalein Atoll, Republic of the Marshall Islands, in the tropical central Pacific. The aircraft involved were based on Kwajalein. A detailed description of the overall experiment and its objectives can be found in Yuter et al. (2005). We are primarily concerned here with the observations from the Convair-580, a four-engine turboprop research aircraft, owned and operated by the Department of Atmospheric Sciences of the University of Washington. The payload included a cloud physics package and a pair of microwave radiometers (21 and 37 GHz) that viewed upward at a 45° angle to the right of the aircraft yaw axis.

These radiometers are the key to this experiment; they measure the cosmic background and the emission from the atmosphere *above* the aircraft. This is a simpler observation than would be provided by a downward-viewing radiometer that would measure the effect of the atmosphere both above and below the aircraft (with different weights) and would have a variable contribution from the ocean surface. In the absence of an absorber, only the 2.7-K cosmic background, T_{cb}, would be measured by an upward-viewing radiometer. If an absorber is present and its approximate temperature, T, is known, the total optical depth, τ, along the line of sight of the radiometer can be computed.

In the absence of scattering, the observed T_b is given by Chang et al. (1993) as

$$T_b = e^{-\tau}T_{\mathrm{cb}} + (1 - e^{-\tau})T.$$

In rain, at 21 and 37 GHz, there is some scattering present that is included in the radiative transfer calculations, but this equation will serve for conceptual understanding. In particular, if the observed brightness temperature is very small compared to the temperature of the emitter, then the sensitivity to uncertainties in the temperature of the emitter is modest and the observed brightness temperature is determined primarily by τ.

The microwave radiometers were of the Dicke switching type (Janssen 1993). They have 3-dB beamwidths of about 6°. The data were digitized at 1-s intervals. The radiometers were calibrated every 60 s by switching to an internal warm load and by using a noise diode on the reference side of the Dicke switch to simulate a cold target. The high-altitude portions of the flights serve as an external cold reference. Further calibrations of the system were performed away from the aircraft with three different targets: blackbodies at ambient and liquid nitrogen temperatures, and the clear sky. The datasets acquired from these calibration runs and during the high-altitude portions of the flights were used to obtain the calibrated brightness temperatures (T_b). The radiometers have a temperature sensitivity of ~0.5 K, and their calibration accuracy is estimated to be about ±4 K.

The Convair-580 aircraft was equipped with a rather extensive cloud physics suite of instruments. The key instruments for this experiment were the Droplet Measurement Technologies hot wire device, which measured the liquid water content for drops in the 10–40-μm range, and the Particle Measurement Systems 2D cloud (2DC) and precipitation (2DP) probes, which measured the drop size spectra over the ranges of 25 μm to 1 mm and 100 μm to 8 mm in diameter, respectively. The cloud physics payload is discussed in more detail by Rangno and Hobbs (2005).

3. Observations

a. Stratiform case

The Convair-580 successfully executed a spiral down through stratiform precipitation on 23 August 1999. The data from the 21- and 37-GHz upward-viewing radiometers are shown as a function of altitude in Figs. 1 and 2, respectively. In each case, the spiral is divided into four quadrants based on the aircraft position relative to the center of the spiral, and different symbols were used to plot the data accordingly. The brightness temperatures are reasonably constant (particularly for the 37-GHz channel) above the freezing level (4.68 km), indicating little absorption or scattering at these altitudes. However, as the aircraft descended below the freezing level, the brightness temperatures increased rapidly with decreasing altitude, indicating significant absorption (and emission) of 21- and 37-GHz radiation. There is some quasiperiodic variation superimposed on the increase of brightness temperature as the aircraft spiraled downward through inhomogeneities in the rain field. The peaks of the variation were consistently in the

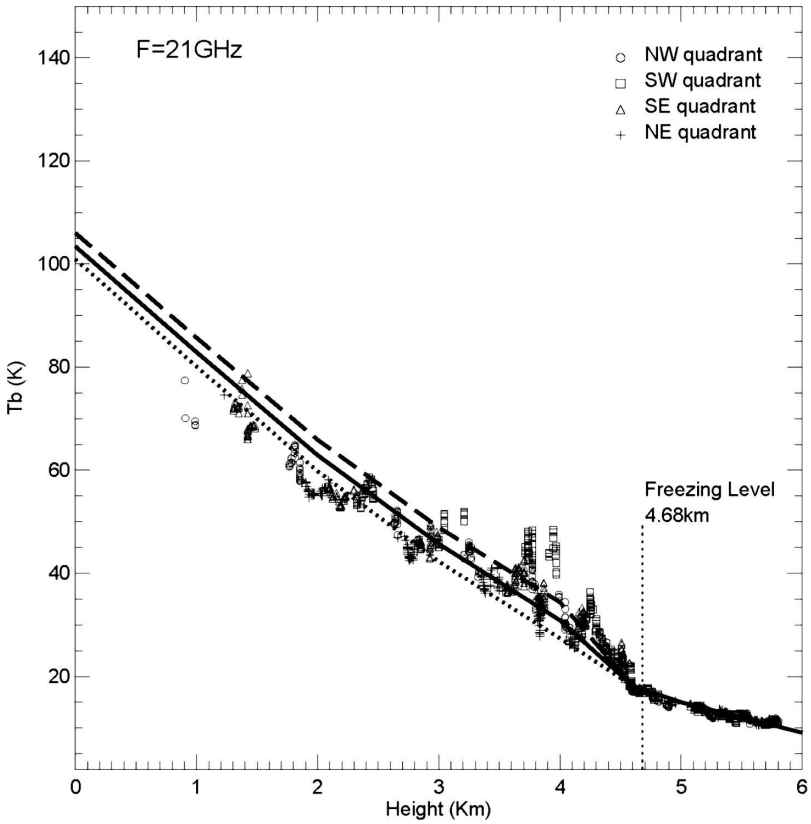

FIG. 1. A comparison of the observed and model-calculated brightness temperatures at 21 GHz as a function of altitude. The observations are characterized according to the quadrant in which the aircraft is located relative to the center of the spiral. The dotted line represents computations with the 500 m below the freezing level treated at face value, the solid line represents calculations for which the absorption and scattering coefficients are doubled for the 500 m below the freezing level, and the dashed line represents tripled absorption and scattering coefficients.

southwest (SW) quadrant and the troughs in the northeast (NE) quadrant, indicating that the quasiperiodic variation was primarily caused by the horizontal inhomogeneity of the rainfall through which the aircraft was spiraling. There were no radar observations suitable for the detection of a bright band, but there was, nevertheless, a melting layer just below the freezing level.

To compute the expected brightness temperature through the profile, we need to characterize the absorbers and scatterers. Figure 3 shows the drop size distribution observed just below the bright band. Measurements from both the 2DP and 2DC probes are shown. The two probes do not give consistent results in this case, underscoring the difficulty of airborne drop size distribution measurements. For reference, the straight lines indicate Marshall and Palmer (1948) distributions for various rain rates. Integration of the DSD observed by the 2DC probe over the fall speed as a function of drop size (Beard 1985) yields a rain rate of 1.3 mm h^{-1}. The 2DP observations suggest an order of magnitude greater rain rate that would be inconsistent with the radiometric observations. The Marshall–Palmer distribution corresponding to 1.3 mm h^{-1} and the observed temperature profile (freezing level = 4.68 km) were inserted into the model described by Wilheit et al. (1977) with computational improvements by Tesmer and Wilheit (1998) and Huang (2001). The model is plane-parallel with 20 streams for the diffuse radiation. In the vertical it has 200 layers of 100-m thickness. It is capable of representing arbitrary size distributions of water or ice spheres. The hot wire probe indicated much less cloud water than assumed in the Wilheit et al. (1977) model (0.5 g m^{-3}). Here we have reduced the cloud liquid water by more than an order of magnitude to 0.04 g m^{-3} to be consistent with the hot wire measurements. With this value, the cloud liquid water has no significant impact on the radiative transfer computa-

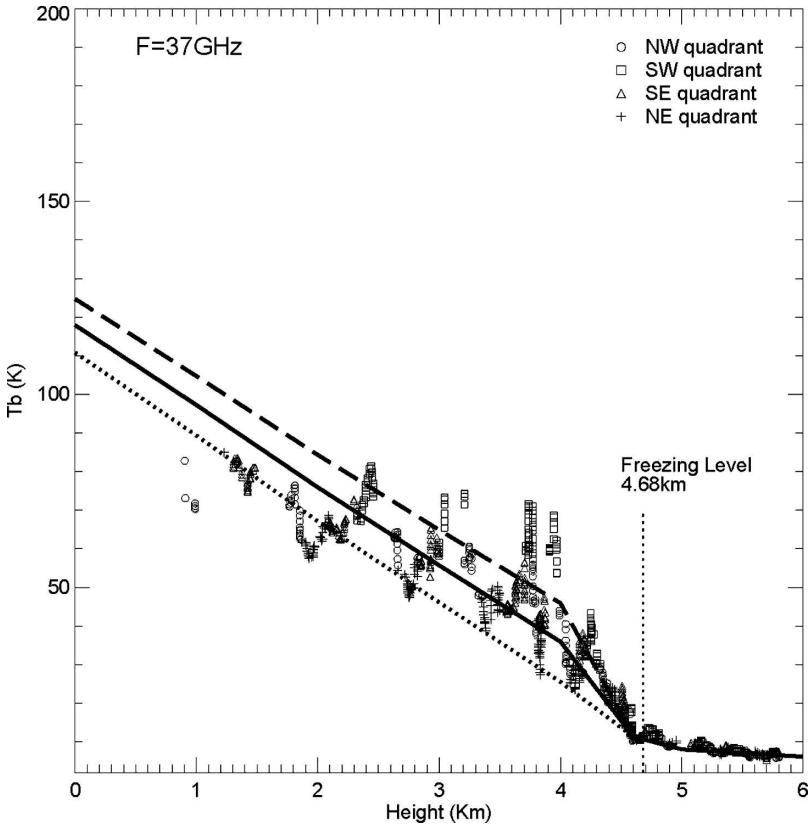

FIG. 2. Same as in Fig. 1, but at 37 GHz.

tions. No hydrometeors were included above the freezing level.

The expected brightness temperatures were computed with the model as described above. The computational code iteratively solved the equation of radiative transfer with scattering and generally converged within two iterations. The results are given as the dotted curves in Figs. 1 and 2. In both cases, the fit above the freezing level is extremely good. This supports the decision to leave out all hydrometeors above the freezing level; water vapor and molecular oxygen are sufficient to account for the observed brightness temperatures. While snow is obviously present above the freezing level, it is not sufficiently opaque to matter in the radiative transfer. In the first kilometer below the freezing level, the computed brightness temperatures are below the observations for both frequencies. With decreasing altitude, the agreement gets better in both cases, but the scatter in the observations also becomes much larger than in the melting layer.

If the absorption and scattering coefficients of the hydrometeors are doubled ($\times 2$) or tripled ($\times 3$) for 0.5 km below the freezing level, as suggested by the modeling results previously discussed, the solid ($\times 2$) and dashed ($\times 3$) curves in Figs. 1 and 2 result. For both frequencies, the fit is improved through the upper part of the rain column with the $\times 2$ computations being near the median of the observations and the $\times 3$ being among the higher brightness temperatures. Through the melting layer, the fit appears best for the $\times 3$ computation. Even larger increases within the melting layer could not be ruled out on the basis of these observations but would not be compatible with the modeling results. The observations are somewhat lower than these computations at the lowest altitudes, but there are many possible sources for this discrepancy, such as the estimate of the average rain rate or the spatial and temporal variability of the rain. The 21-GHz observations are not very sensitive to the hydrometeor assumptions but the 37-GHz observations are quite so.

Chang et al. (1993) report an experiment very similar to the stratiform precipitation observations reported here but in *extratropical* stratiform rain. They spiraled up through stratiform rainfall with uplooking microwave radiometers at the same two frequencies used in KWAJEX (21 and 37 GHz). They examined two

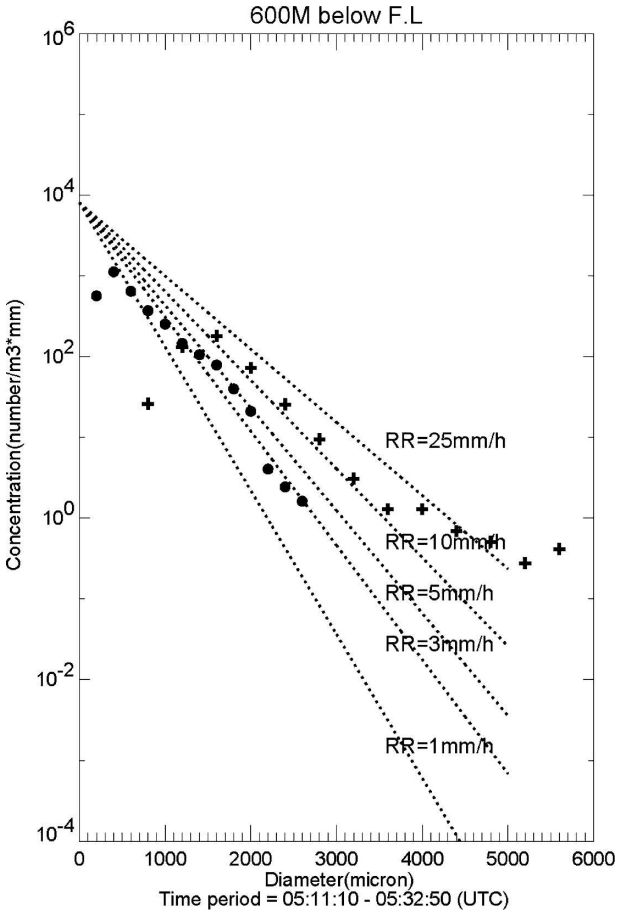

FIG. 3. The measured DSD at about 600 m below the freezing level. The straight lines are the Marshall–Palmer distributions for various rain rates, the dots are observations from the 2DC probe, and the crosses are from the 2DP probe.

cases—1 February 1983 in the North Pacific and 2 March 1983 in the North Atlantic. The rain rates were approximately 8 and 1 mm h^{-1} and the freezing levels were at altitudes of 1.8 and 2.5 km, respectively. There were no radar data in support of their observations. Microphysics observations, in the form of PMS particle probes, were available only for the 2 March case. In neither case did they attribute any additional absorption to brightband effects. However, on examining their data, enhanced absorption in the 0.5 km below the freezing level is quite obvious in the 2 March case but not in the 1 February case. They accounted for this enhancement with a layer of nonprecipitating cloud with modest support from the PMS probes. Since the rain rate was very low ($\sim$1 mm h^{-1}), either explanation will work. For the 1 February case, the larger rain rate masked the impact of the same nonprecipitating cloud assumption and there was no apparent enhancement of the absorption in the melting layer.

b. Convective case

On 11 August 1999, the Convair-580 flew back and forth along a line penetrating convective rain at levels of 2.6, 3.4, and 4.5 km. This last flight leg (4.5-km altitude) was only 100 m below the freezing level (4.6 km). The 37-GHz data for the 4.5-km altitude line, covering a distance of about 37 km, are shown in Fig. 4. There is a high degree of variability along the line as the aircraft flew through rainfall of varying intensity. The horizontal lines in the figure represent computations from the Wilheit et al. (1977) model for various rain rates. These computations assume a liquid layer thickness of only 100 m above the aircraft. Clearly, there is a significant amount of opacity (potentially supercooled water) above the flight altitude.

Since at the frequencies considered here, the absorption coefficient is approximately linear in the rain rate, we can characterize the rain signal as a vertically integrated rain rate (VIR) where the integral is over the liquid portion only. The corrections due to the temperature profile and scattering, while nonzero, are of lesser significance. The rain rate for this integral is the *apparent* rain rate as represented by the microwave radiance. Supercooled water not properly accounted for would make the apparent rain rate higher than the true rain rate. The brightness temperature associated with a given VIR depends on the observation frequency, polarization, and viewing geometry. Thus we will try to estimate the impact of supercooled water by comparing the increment of VIR contributed by supercooled water to the total VIR. The VIR is conceptually similar to the total overburden of liquid water. However, by expressing it as rain rate, the sensitivity to drop size distribution more closely reflects that of the absorption coefficient as discussed in Wilheit et al. (1977). Moreover, in the presence of varying rain rates, the absorption coefficient is not linearly related to liquid water content as it is to rain rate.

Since the peak brightness temperature in the 4.5-km data corresponds to 20 mm h^{-1} over a 0.1-km thickness, the increment of VIR above this altitude would be $\sim$2 m^2 h^{-1}. This is an upper limit to the total impact of supercooled water since some, though probably not all, of the water is in the first 100 m above the aircraft and therefore above freezing. To estimate how much of the liquid overburden is supercooled, we need to estimate the thickness of the liquid water layer above the aircraft. Given that the observed brightness temperatures determine the VIR with little uncertainty, an estimate of the average rain rate over the layer yields, in turn, an estimate of its thickness. Thus, over the next few paragraphs, we will marshal the available evidence to de-

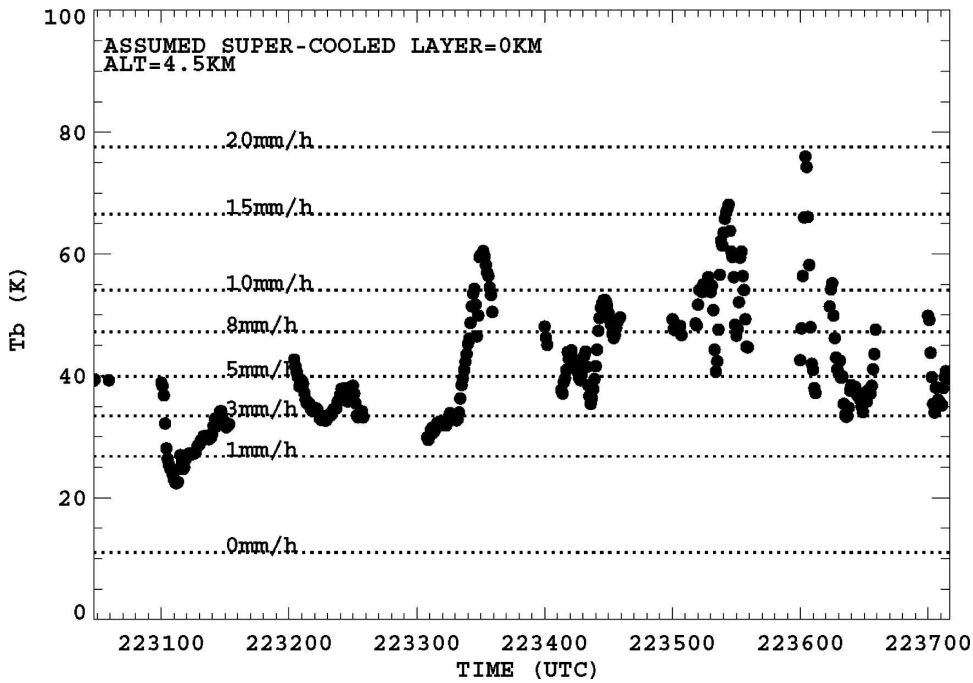

FIG. 4. The brightness temperature variations along a flight segment at a constant altitude of 4.5 km, about 100 m below the freezing level. The horizontal lines are calculated brightness temperatures based on the model of Wilheit et al. (1977) for various rain rates.

termine the reasonable range of rain rates above the aircraft so that estimates of the supercooled contribution can be constrained. We will also estimate the VIR over the entire column to elucidate the impact of any supercooled water on a rain-rate retrieval.

The key to estimating the total VIR in the convective cores is to choose a proper rain rate within the raining layer. The rain rate should be representative of the rain rates found below the freezing level. At the simplest level, one might rely on conventional wisdom and assign a rain rate on the order of 25 mm h^{-1} (1 in. h^{-1}) to the convective rain (VIR $\sim$ 115 m^2 h^{-1}). Over the ocean, variations by up to a factor of 2 would be common, and somewhat larger variations are certainly possible. This estimate establishes a credible range for more quantitative estimates. Here, estimates based on the observed DSD, on ground-based radar, and on the microwave radiances will all be examined.

Figures 5, 6, and 7 show the drop size distributions measured by the PMS 2DP and 2DC probes on the Convair-580 as the aircraft penetrated the convection at altitudes of 2.6, 3.4, and 4.5 km. Superimposed on these measured distributions are lines representing Marshall–Palmer distributions for various rain rates. The distribution at 2.6 km is reasonably consistent with a rain rate of 25 mm h^{-1} and at 3.4 km with a rain rate of 10 mm h^{-1}. At 4.5 km (immediately below the freezing level), the observed drop size distribution is not consistent with any Marshall–Palmer distribution. The general decrease of rain rate with height suggests warm rain processes. On the other hand, the large number of large particles at 4.5 km suggests that some snowflakes are to be found at this level. Clearly, many processes are at work on this 37-km-long, nominally convective flight line.

The drop size distribution data are consistent with rain rates on the order of 10–25 mm h^{-1} in the convection. If we take the estimate from 2.6 km as the average through the column, a VIR of about 115 m^2 h^{-1} results again. If, on the other hand, we assume that the rain rate is constant below the 2.6-km line but decreases more or less linearly up to the freezing level as suggested by the 3.4-km data, we would get a VIR of about 90 m^2 h^{-1}.

An examination of the ground-based radar data from Kwajalein (KWAJEX 1999) for 2213 UTC (early in the penetrations) and 2237 UTC (late in the penetrations) shows echoes for the convective cores in the 37.5–42.5-dBZ range but none greater than 42.5 dBZ. Using the Z–R relationship for a Marshall–Palmer distribution ($Z = 200R^{1.6}$) yields a rain-rate range of 8–16 mm/h for the 37.5–42.5-dBZ range. Thus, the radar suggests somewhat lower rain rates than do the DSD data. Other Z–R relationships are possible, but they would not materially change the conclusion that the maximum rain

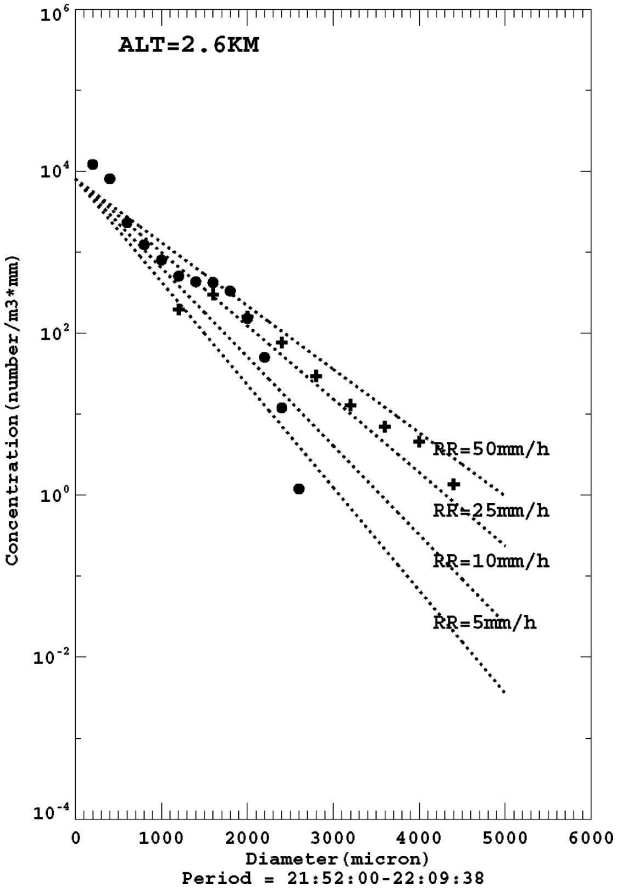

FIG. 5. The DSDs measured at the 2.6-km altitude in a convective rain system. The straight lines represent the Marshall and Palmer (1948) distributions for various rain rates, the dots are observations from the 2DC probe, and the crosses are from the 2DP probe.

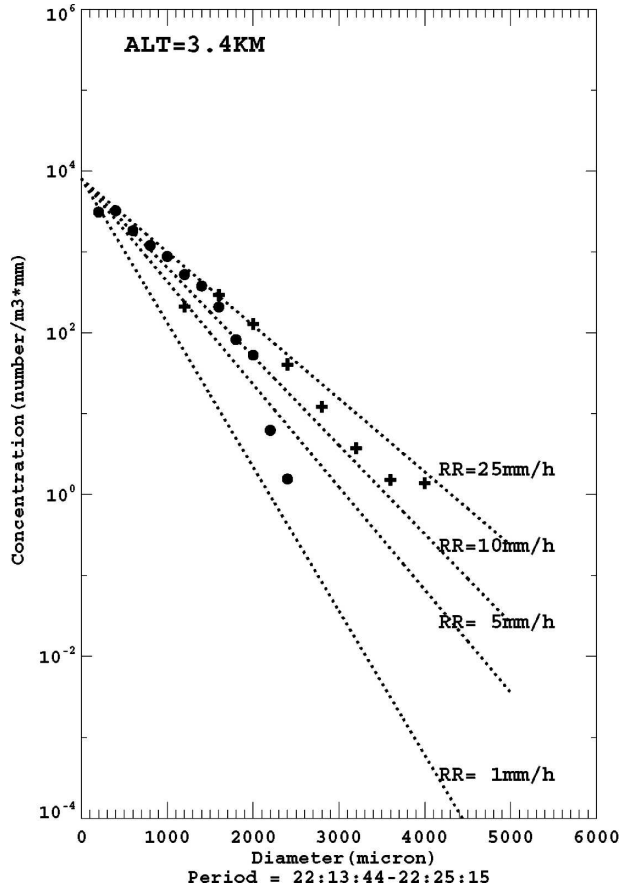

FIG. 6. Same as in Fig. 5, but at the 3.4-km altitude.

rates are on the order of 10–25 mm h^{-1} (VIR ~ 50–100 m^2 h^{-1}).

For each aircraft flight altitude, brightness temperature–rain-rate relationships were computed for the two channels of the microwave radiometer assuming various thicknesses of the supercooled water layer. The observed brightness temperatures were interpreted in terms of rain rates using these relationships. Since we are interpreting in terms of VIR, the inclusion of vertical rain-rate variability is not necessary although the model is capable of handling an arbitrary vertical structure. Figure 8 shows the statistics of these rain rates as cumulative percentiles assuming 0-, 0.1-, 0.25-, and 0.5-km supercooled water layer thicknesses as calculated from the 37-GHz data. The rain rate so calculated represents the average rain rate from the aircraft altitude to the freezing level plus the supercooled water thickness. The supercooled water layer only has a modest impact on the interpreted rain rates for the 2.6-km altitude data. The rain rates observed from this altitude range up to about 25 mm h^{-1} in general agreement with rain rates inferred by other means. At the 3.4-km altitude, the inferred rain rates are generally lower. If no supercooled water is assumed (layer thickness = 0 km), the maximum rain rate is around 10 mm h^{-1}, indicating some decrease with altitude as was inferred from the DSD data. A working value of 100 m^2 h^{-1} for the total VIR in the convective cores would be reasonable given all the available observations so that the contribution to the VIR from above 4.5-km altitude is about 2% of the total. Since the freezing level is 100 m higher, this represents an upper limit to the supercooled water contribution.

How much of the 2% VIR from above the flight level is supercooled is another question. Including some supercooled water in the radiative transfer model decreases the interpreted rain rates; at a 0.5-km supercooled water layer thickness, the maximum rain rate observed from 3.4 km is less than 5 mm h^{-1}. The observations at 4.5 km are, of course, the most sensitive to the layer thickness assumption. If we assume no super-

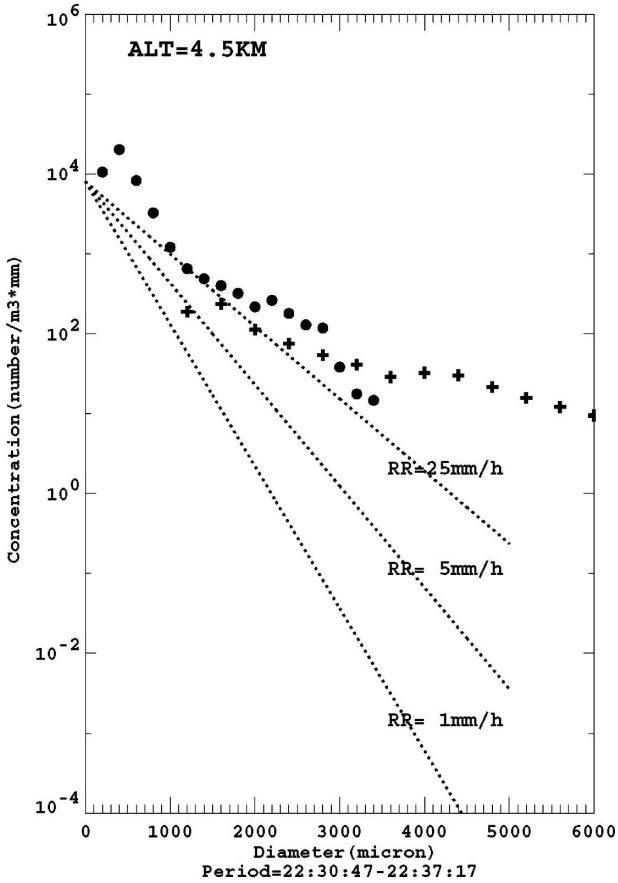

FIG. 7. Same as in Fig. 5, but at the 4.5-km altitude.

cooled water, the 4.5-km rain rates lay between the 3.4- and 2.6-km rain rates with a maximum around 20 mm h^{-1}. At an assumed supercooled water layer thickness of 0.1 km, the statistics of the 3.4- and 4.5-km rain rates are virtually identical. Thicker supercooled water layers decrease the rain rates still further. If we accept the 0.0- or 0.1-km supercooled water thickness computations, then the 4.5-km rain rates break the vertically decreasing rain-rate pattern. The 0.25- and 0.5-km computations produce a more consistent pattern in the vertical. This (admittedly very indirect) reasoning suggests that more than half of the 2% VIR contribution is supercooled. Other rain or cloud distributions between the aircraft altitude and the temperature of spontaneous nucleation (233 K) could also reproduce the observed brightness.

We have ignored any scattering by ice above the freezing level that would increase the brightness temperature in this upward-viewing geometry by scattering the relatively high upwelling brightness temperatures back down to the radiometer. Thus, some of the brightness temperature increases may have been contributed by ice so that the contribution by supercooled liquid would be even smaller than we have estimated. Ice was not included in the calculations, as there were no observations to constrain the ice assumptions.

The 21-GHz data are not shown. There was a calibration shift during the 2.6-km line, invalidating part of those data, and there was insufficient sensitivity to hydrometeors (due to the lower frequency) to provide much information from the 4.5-km flight line. The 21-GHz observations are not inconsistent with the 37-GHz observations, but given the shortcomings, they add no new insights.

4. Conclusions

Based on the example discussed here, the microwave attenuation in the mixed-phase region just below the freezing level in stratiform rain appears to be roughly doubled or tripled for the 0.5 km below the freezing level. The stratiform rain observations, while consistent with the range of the modeling results, are not sufficient to constrain the modeling. Even more attenuation in the melting layer than what is predicted by the models would be consistent with the observations but less attenuation would not be. These observations contrast with the two examples given by Chang et al. (1993), where no extra attenuation was reported (one case is debatable). In the Chang et al. (1993) examples, there was no verification of the presence of a bright band, although the presence of such a band would seem likely under the circumstances. In any case, from a passive microwave rainfall retrieval algorithm point of view, the key observation is that sometimes there is extra attenuation and sometimes not. It is possible that the seasonal/regional differences among the three observations could account for the attenuation differences. For the present, this must be left unknown.

Similarly, the possible emission of microwave radiation by the supercooled water in a convective updraft has been noted. The excess attenuation/emission caused by supercooled water in this case is no more than 2% of the total in the updrafts. It is possible that this example is an extreme case; more supercooled water could be commonplace. However, this is the only observation in hand and aircraft safety and operational concerns make obtaining more data difficult.

The uncertainty in the retrievals is an important issue. There are many factors that contribute to the uncertainty, and this contribution is not the largest by any means except at very low freezing levels where the melting layer becomes a large fraction of the total rain column. It appears that the uncertainty in the attenuation in the melting layer is about a factor of 3, ranging

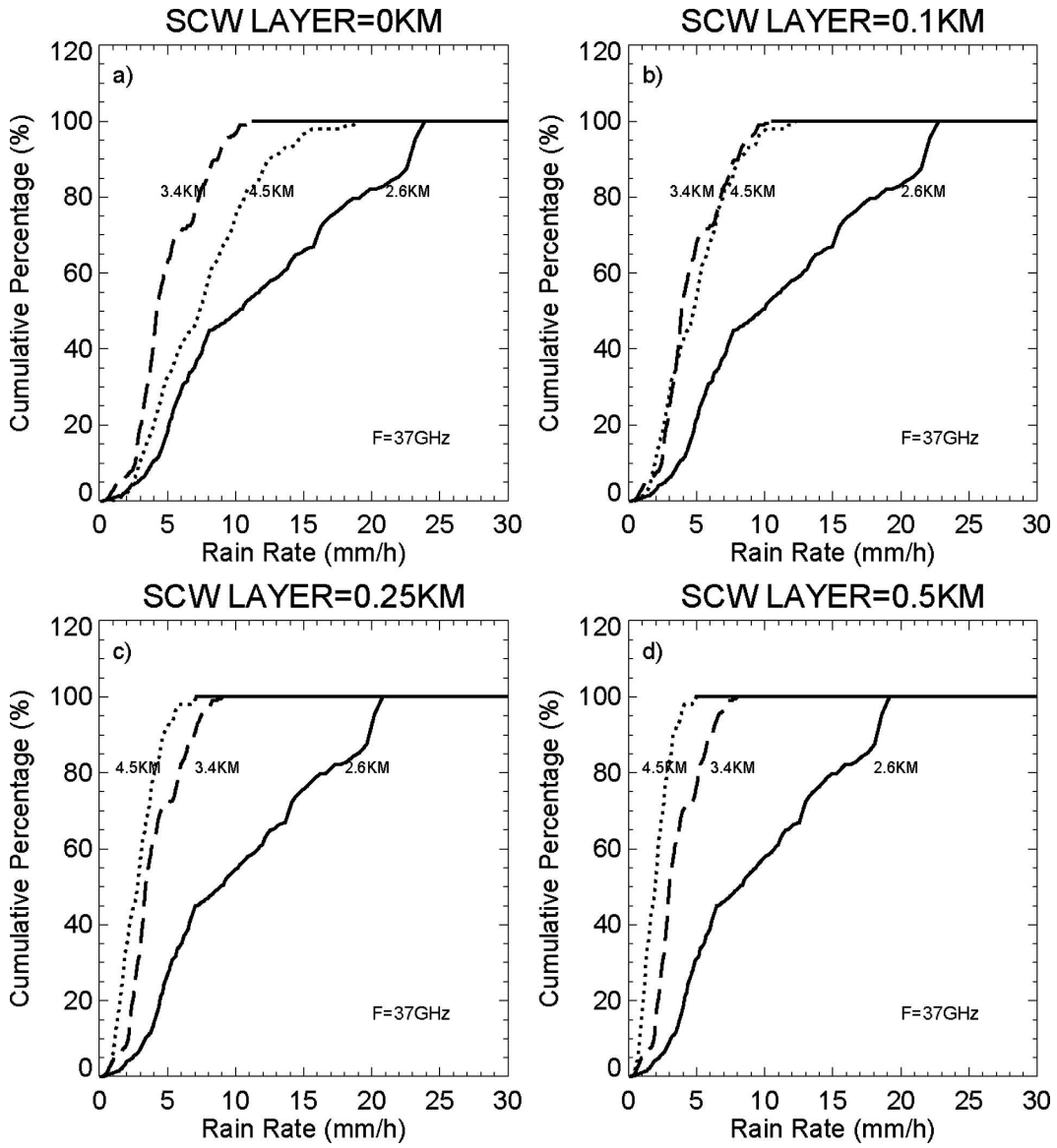

FIG. 8. Cumulative probabilities of rain rates inferred from 37-GHz brightness temperatures along three flight lines at constant altitudes of 2.6 (solid line), 3.4 (dashed line), and 4.5 km (dotted line). The computations were carried out for assumed supercooled liquid water layer thicknesses of 0, 0.1, 0.25, and 0.5 km.

from equal to the attenuation of the rain below to perhaps 3 times that value. While there is significant uncertainty in the modeling of the melting layer, the natural variability appears to be larger. More data might allow us to understand the sources of this variability and to account for it. The one case we have here does not enable us to make any useful statements about the uncertainty due to supercooled water in the convective updrafts.

Clearly, it is important to get more observations so that the statistics as well as the regional and seasonal components of the mixed phase can be more clearly defined. Upward-viewing radiometers on aircraft provide a fairly direct measure of the attenuation, but it is difficult to observe many cases this way. Inhomogeneities and the realities of aircraft operation further compound the difficulty of this approach. However, attenuation can also be inferred from multifrequency radars. An airborne radar, such as the recently modified Airborne Rain Mapping Radar (ARMAR; Sadowy et al. 2003), is able to collect more cases rapidly; data from this instrument are just now becoming available, but selection bias in aircraft observations is always a concern. A truly global set of statistics could be gained

from a multifrequency spaceborne radar, such as that proposed for the Global Precipitation Mission.

Acknowledgments. The authors gratefully acknowledge the financial support of the NASA TRMM project and NSF for this research. They likewise acknowledge useful, insightful, and provocative comments by anonymous reviewers.

REFERENCES

Bauer, P., 2001: Including a melting layer in microwave radiative transfer simulation for clouds. *Atmos. Res.,* **57,** 9–30.

——, J. P. V. Poiares Baptista, and M. de Iulis, 1999: The effect of the melting layer on the microwave emission of clouds over the ocean. *J. Atmos. Sci.,* **56,** 852–867.

——, A. Khain, A. Pokrovsky, R. Meneghini, C. Kummerow, F. Marzano, and J. P. V. Poiares Baptista, 2000: Combined cloud-microwave radiative transfer modeling of stratiform rainfall. *J. Atmos. Sci.,* **57,** 1082–1104.

Beard, K. V., 1985: Simple altitude adjustments to raindrop velocities for Doppler radar analysis. *J. Atmos. Oceanic Technol.,* **2,** 468–471.

Chang, A. T. C., A. Barnes, M. Glass, R. Kaker, and T. T. Wilheit, 1993: Aircraft observations of the structure of stratiform precipitation relevant to microwave radiative transfer. *J. Appl. Meteor.,* **32,** 1083–1090.

——, L. S. Chiu, C. Kummerow, J. Meng, and T. T. Wilheit, 1999: First results of the TRMM Microwave Imager (TMI) monthly oceanic rain rate: Comparison with SSM/I. *Geophys. Res. Lett.,* **26,** 2379–2382.

Huang, J., 2001: An algorithm for retrieval of monthly rainfall over the oceans from the TRMM Microwave Imager (TMI). Ph.D. dissertation, Dept. of Atmospheric Sciences, Texas A&M University, 93 pp.

Iguchi, T., T. Kozu, R. Meneghini, J. Awaka, and K. Okamoto, 2000: Rain-profiling algorithm for the TRMM precipitation radar. *J. Appl. Meteor.,* **39,** 2038–2052.

Janssen, M. A., Ed., 1993: *Atmospheric Remote Sensing by Microwave Radiometry*. John Wiley and Sons, 572 pp.

Kawanishi, T., and Coauthors, 2003: The advanced microwave scanning radiometer for the earth observing system (AMSR-E), NASDA's contribution to the EOS for global energy and water cycle studies. *IEEE Trans. Geosci. Remote Sens.,* **41,** 184–194.

Kummerow, C., W. Barnes, T. Kozu, J. Shiue, and J. Simpson, 1998: The Tropical Rainfall Measuring Mission (TRMM) sensor package. *J. Atmos. Oceanic Technol.,* **15,** 809–817.

——, and Coauthors, 2001: The evolution of the Goddard Profiling Algorithm (GPROF) for rainfall estimation from passive microwave sensors. *J. Appl. Meteor.,* **40,** 1801–1820.

KWAJEX, cited 1999: KWAJEX radar images. [Available online at http://www.atmos.washington.edu/kwajex/ops-web/radar/.]

Liang, L., and R. Meneghini, 2005: On modeling air/space-borne radar returns in the melting layer. *IEEE Trans. Geosci. Remote Sens.,* **43,** 2799–2809.

Marshall, T. S., and W. M. Palmer, 1948: The distribution of raindrops with size. *J. Meteor.,* **5,** 165–166.

Olson, W. S., P. Bauer, N. F. Viltard, D. E. Johnson, W. K. Tao, R. Meneghini, and L. Liao, 2001a: A melting-layer model for passive/active microwave remote sensing applications. Part I: Model formulation and comparison with observations. *J. Appl. Meteor.,* **40,** 1145–1163.

——, ——, C. D. Kummerow, Y. Hong, and W.-K. Tao, 2001b: A melting-layer model for passive/active microwave remote sensing applications. Part II: Simulation of TRMM observations. *J. Appl. Meteor.,* **40,** 1164–1179.

Rangno, A. L., and P. V. Hobbs, 2005: Microstructures and precipitation development in cumulus and small cumulonimbus clouds over the warm pool of the tropical Pacific Ocean. *Quart. J. Roy. Meteor. Soc.,* **131,** 639–673.

Sadowy, G. A., A. C. Berkun, W. Chun, E. Im, and S. L. Durden, 2003: Development of an advanced airborne precipitation radar. *Microwave J.,* **46,** 84–98.

Tesmer, J. R., and T. T. Wilheit, 1998: An improved microwave radiative transfer model for tropical oceanic precipitation. *J. Atmos. Sci.,* **55,** 1674–1689.

Wilheit, T. T., A. T. C. Chang, M. S. V. Rao, E. B. Rodgers, and J. S. Theon, 1977: A satellite technique for quantitatively mapping rainfall rates over the oceans. *J. Appl. Meteor.,* **16,** 551–560.

——, C. D. Kummerow, and R. Ferraro, 2003: Rainfall algorithms for AMSR-E. *IEEE Trans. Geosci. Remote Sens.,* **41,** 204–214.

Yuter, S. E., R. A. Houze Jr., E. A. Smith, T. T. Wilheit, and E. Zipser, 2005: Physical characterization of tropical oceanic convection observed in KWAJEX. *J. Appl. Meteor.,* **44,** 385–415.